ACS Sustainable Chemistry & Engineering

Research Article

pubs.acs.org/journal/ascecg

Effect of Ni Particle Location within the Mesoporous MCM-41 Support for Hydrogen Production from the Catalytic Gasification of Biomass

Chunfei Wu,*[,†] Lisha Dong,[‡] Jude Onwudili,[†] Paul T. Williams,*[,†] and Jun Huang*[,‡]

[†]Energy Research Institute, The University of Leeds, Leeds, LS2 9JT, U.K.

[‡]Laboratory for Catalysis Engineering, School of Chemical and Biomolecular Engineering, The University of Sydney, NSW 2006, Australia

ABSTRACT: Thermal processing of biomass in the presence of a catalyst is a promising technology to generate H_2-rich gases for fuelling the future. Metal particles loaded on porous supports have been widely used for biomass gasification. However, no detailed research has been designed for describing the catalytic performance of nickel particles located inside compared to outside the pores of the supports. In this work, two groups of Ni/MCM-41 catalysts were prepared: I-series catalysts where most of the NiO particles were located inside the mesopores of MCM-41 and O-series catalysts where most of the NiO particles were located outside the pores of MCM-41. The prepared catalysts were used in the pyrolysis-catalytic gasification of wood sawdust using a two-stage fixed-bed reaction system. Gasification on the I-series catalysts generated more gas and hydrogen and lower oil, compared with the O-series catalysts. Hydrogen production was increased from 16.46 to 21.26 (mmol H_2 g^{-1} wood) when the catalyst was changed from 20%Ni−O to 20%Ni−I. The better performance of the I-series catalysts in relation to hydrogen production is suggested to be due to the longer residence time of pyrolysis reactants inside the pores of the MCM-41 and thus a longer contact time between reactants and active Ni sites. In addition, the high dispersion of the fine NiO particles inside the pores of the MCM-41 support enhances the catalytic performance of the I-series catalyst during the pyrolysis/gasification of biomass.

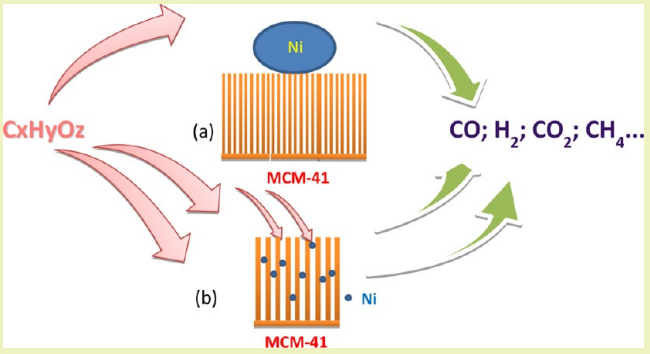

KEYWORDS: *Nickel, Wood sawdust, Pyrolysis, Gasification, MCM-41, Hydrogen*

INTRODUCTION

Hydrogen is regarded as one of the most clean and renewable energies for the future;[1,2] as hydrogen can be used for green technologies such as fuel cell applications with high efficiency[3,4] and the combustion product of hydrogen is only water. Currently, ~96% of hydrogen is produced from steam reforming of natural gas.[5] To reduce the dependence on fossil fuels and their associated environmental impact, renewable resources for hydrogen production are of great interest.

Biomass is an abundantly available natural resource, and most importantly, it is a reliable, renewable, clean, and carbon-neutral energy resource. It has been reported that around 6% of primary energy production is shared by biomass and municipal solid wastes in the EU in 2009, and for some EU countries the share is close to 20% (Finland and Sweden).[6] In addition, biomass has the potential to make a valuable contribution to the reduction of greenhouse gas emissions, for which some regions and countries have set ambitious targets. For example, the EU has set a target for the reduction in greenhouse gas emission of at least 20% below 1990 levels by 2010,[7] and the U.K. is committed to have at least 60% cuts in CO_2 emissions by 2050.[8]

Gasification of biomass to produce an H_2 rich syngas has been investigated as a promising alternative to fossil fuel hydrogen generation.[9−11] One of the key challenges is to obtain suitable catalysts for the process of biomass gasification in relation to the improvement of the efficiency of hydrogen production and biomass conversion. Nickel-based catalysts have been widely used for hydrogen production from catalytic steam reforming of bio-oil compounds, with comparable catalytic activity compared with noble metal (Pt, Ru, and Rh) catalysts[12−15] and at relatively low cost. However, Ni-based catalysts suffer more coke deposition and sintering problems compared with noble metal catalysts.[13,16]

The type of support of the catalyst plays an important role in the catalytic activity of Ni-based catalysts. There have been extensive investigations of different catalyst supports such as Al_2O_3,[17,18] MgO,[19] CeO,[20] zeolite,[21] etc. For example, several Ni-based catalysts (10 wt % Ni) with different supports have been studied for hydrogen production from pyrolysis/gas-

Received: November 2, 2012
Revised: June 21, 2013
Published: June 28, 2013

dx.doi.org/10.1021/sc300133c | ACS Sustainable Chem. Eng. 2013, 1, 1083−1091

ification of polypropylene.[22] It was found that a Ni/ZSM-5 catalyst with comparatively higher surface area generated higher gas and hydrogen production compared with Ni/MgO and Ni/Al_2O_3 catalysts; however, faster catalyst deactivation related to coke formation was obtained for the reacted Ni/ZSM-5 catalyst. Superior catalytic activity related to hydrogen production from cellulose gasification has been reported for a Ni-based catalyst with MCM-41 as the support compared with an Al_2O_3 support;[23] the authors suggesting that this was due to the highly ordered mesoporous structure of the MCM-41 support improving Ni dispersion and thus increasing interactions between Ni sites and gaseous molecules. Various catalyst supports with 10 wt % Ni have been investigated for hydrogen production from the gasification of cellulose.[24] It was reported that Ni/metal oxides were found to favor tar production, while Ni/zeolite catalysts could reduce the formation of tar, but generated more coke. In addition, the authors also proposed that Ni crystallite size was not significantly affected by the type of catalyst support and that catalysts with Ni crystallite sizes of around 25 nm generated the highest hydrogen production.[24]

The two main types of nickel-based catalyst supports reported above have been porous materials and metal oxides, and the conclusions suggest that porous materials have advantages of tar reduction and higher hydrogen production compared with the metal oxides. However, the problem of coke deposition for the Ni-porous type catalysts is more serious. Furthermore, Ni/porous type catalysts (e.g., Ni/ZSM-5) have also been reported to have lower hydrogen production compared with Ni−Al catalysts during the catalytic gasification of plastics.[22] Therefore, more detailed investigations of Ni-porous type catalysts are needed to improve the catalyst performance related to hydrogen production and catalyst stability. For example, the Ni metal dispersion on the surface of the catalyst and the pore structure of the pores of the support are interesting areas of research. The pore size of the catalyst support has been reported to be essential for biomass gasification, as it has been shown that ZSM-5 zeolite with smaller pore size than ZY-30 zeolite produced lower catalytic activity for the reduction of biomass tars.[25] Increasing the pore size of catalysts has also been reported to improve catalyst performance during the catalytic cracking of heavy oils.[26]

MCM-41 is a porous material with high surface area (~1000 $m^2\ g^{-1}$), wide range of pore diameters (2−10 nm), and flexible structure of the amorphous silica wall and has been used widely for reactions such as oxidation, polymerization, and reforming.[27−29] Due to the porous structure of the MCM-41 material, the interaction and relation between Ni metals and support are important for catalytic performance during the steam reforming of hydrocarbons. There have been studies on the relation of Co metals with MCM-41 pore structure. For example, the incorporation of Co metal or Co oxides into the molecular sieves of MCM-41 was reported to increase the catalyst performance in relation to catalyst sintering during reforming reactions.[30,31] In addition, the size of metal clusters has been reported to be strongly influenced by the pore size of the MCM-41 support, the larger pores of MCM-41 resulting in larger metal particles.[31−33] The study of Ni/MCM-41 catalysts during biomass gasification has shown that the size of NiO particles was increased and the NiO particles were found to move from inside of the pores of the MCM-41 to outside the pores when the Ni loading was increased from 5 to more than 20 wt %.[23,34] Gas and hydrogen productions were reduced during the biomass gasification when bulky NiO particles were observed outside the MCM-41 support compared with the Ni/MCM-41 catalyst with only NiO particles inside the pores.[23] However, gas and hydrogen productions were increased during a two-stage pyrolysis/gasification of biomass, when the location of NiO was shifted from inside the pores of the support to both inside and outside the support with an increase of the Ni loading.[34] Therefore, it is not clear whether NiO particles located outside the pore of the MCM-41 support is beneficial for hydrogen production from biomass gasification compared with NiO particles located inside the pores of the support.

Furthermore, as mentioned previously, Ni-based catalysts with porous supports have a more serious coke deposition problem compared with Ni/metal oxides catalysts. In addition, the location of NiO particles on the surface of the MCM-41 support has also shown influence on the coke deposition after biomass gasification.[34] Therefore, investigation of the relationship between Ni metal oxides and the porous support with a full analysis of the gas and oil products is desirable for the design of suitable porous Ni-based catalysts able to maximize hydrogen production and minimize coke formation during biomass gasification.

Here, we prepared Ni/MCM-41 catalysts with NiO particles located in different areas of the MCM-41 support. The influence of NiO location on hydrogen production and coke formation have been investigated in relation to biomass gasification by using a two-stage fixed bed reaction system.

MATERIALS AND METHODS

Materials. Wood sawdust was used with a particle size of less than 0.2 mm with a moisture content of 6.4 wt %, volatile content of 74.8 wt %, fixed carbon content of 18.3 wt %, and ash content of 1.2 wt %.

The MCM-41 support was prepared according to the procedures reported by Cheng et al.[35] The catalyst with NiO particles purposely located outside the pores of the MCM-41 support was assigned as 10%-O and 20%-O for the Ni loading of 10 and 20 wt %, respectively. The Ni/MCM-41 catalyst with NiO loaded inside the pores of the MCM-41 support was assigned as 10%Ni−I and 20%Ni−I, respectively. All Ni/MCM-41 catalysts were prepared by an impregnation method. Initially, the required amount of Ni-$(NO_3)_2{\cdot}6H_2O$ (Sigma−Aldrich) was dissolved in ethanol (99%, Sigma−Aldrich) to form a 1 mol/L of solution. Then, impregnation was employed by addition of powdered MCM-41 to the nickel precursor solution. The mixture was stirred for 30 min for O-series catalysts and for 2 h for I-series catalysts, respectively. The nickel nitrate particles were dissolved and attached on the external surface of the MCM-41 support by stirring for 30 min; while longer stirring time (2 h) enables the nickel nitrate particles to diffuse into the pores of the MCM-41 support. The evaporation of the mixture was carried out at 80 °C, the obtained solids were calcined in a muffle furnace at 550 °C for 4 h with a heating rate of 1 °C min^{-1} in the presence of static air.

Pyrolysis-Gasification of Wood Sawdust. The biomass gasification experiments were carried out in a two-stage fixed-bed reaction system, which has been reported in our previous work.[34] Biomass wood sawdust was pyrolyzed in a first reactor, the derived gaseous pyrolysis products are passed directly to a second reactor where catalytic steam gasification takes place. For each experiment, about 0.8 g wood sawdust and 0.25 g catalyst or sand were used. The pyrolysis and gasification temperatures were 530 and 800 °C, respectively. Initially, the catalyst bed was heated and stabilized at 800 °C; the sample located in the pyrolysis stage was then started to be heated to 530 °C with a heating rate of 40 °C min^{-1}; water was started to be injected when the pyrolysis temperature was about 200 °C. N_2 was used as carrier gas for each experiment. The derived gaseous products were condensed with dry ice cooled condensers to produce the liquid

products and the noncondensed gases were collected with a Tedlar gas sample bag for further analysis.

Analysis of Gas and Oil from Gasification. The noncondensed gases were analyzed off-line by gas chromatography (GC). CO, H_2, and N_2 gases were determined by a Varian 3380 GC on a 60−80 mesh molecular sieve column with argon carrier gas. The CO_2 gases was analyzed by another Varian 3380 GC on a Hysep 80-100 mesh column with argon carrier gas. C_1−C_4 hydrocarbons were detected using a further Varian 3380 GC with a flame ionization detector with N_2 as carrier gas.

The liquid products collected by the condensers from the pyrolysis/gasification of wood sawdust were rinsed with wash-agent dichloromethane (DCM). The oil fraction in the liquid mixture was separated out and concentrated to a detection level using a Genevac Rocket Evaporation system. The oil fraction composition was then determined using a Varian CP-3800 GC coupled with a Varian Saturn 2200 mass spectrometer (MS). The conditions for the GC/MS equipment were: GC injector port temperature 290 °C; transfer line temperature 280 °C; manifold temperature 120 °C and trap temperature 200 °C; the oven program temperature was 40 °C for 2 min, then it was ramped to 280 °C with 5 °C min^{-1}, and finally held at 280 °C for 10 min. The compounds in the oil were quantified with external standards.

Characterization of Catalysts. The BET surface areas of the fresh catalysts were determined by N_2 adsorption and desorption isotherms on a Quantachrome Autosorb-1. The results for the catalysts with NiO particles inside the pores of MCM-41 have a lower BET surface area (around 450 m^2 g^{-1}) compared with the catalysts with NiO particles outside the pores (around 870 m^2 g^{-1}), while there was no large difference for the catalysts in relation to different Ni loadings. The fresh catalysts were analyzed by X-ray diffraction (XRD) on a Siemens D5000 between 10° and 70° with a scanning step of 0.02° using Cu Kα radiation. The fresh catalysts were also characterized by scanning electron microscopy (SEM; FESEM, Zeiss Ultra+) and transmission electron microscopy (TEM) (Philips CM120). Temperature programmed reduction (TPR) was also used to characterize the fresh catalysts using a Stanton-Redcroft thermogravimetric analyzer (TGA). During the TPR analysis, the fresh catalyst was heated at 20 °C min^{-1} to 150 °C and held for 30 min, then heated at 10 °C min^{-1} to 900 °C in an atmosphere of gas mixture containing 5% H_2 and 95% N_2 (50 mL min^{-1}). The reacted catalysts were analyzed by temperature programmed oxidation using TGA (Shimadzu). The reacted catalyst was heated from room temperature to 800 °C with a heating rate of 15 °C min^{-1} and held for 10 min at 800 °C. The reacted catalysts were also analyzed by SEM (LEO 1530) to obtain information on the deposited carbons on the surface of the catalyst.

RESULTS AND DISCUSSION

Characterization of Fresh Catalysts. The fresh catalysts were characterized by TPR, and the results are shown in Figure 1. The 10%Ni−O and 20%Ni−O catalysts both showed a reduction peak at around 410 °C. The results suggest that large bulky NiO particles were formed on the surface of the 10%Ni−O and 20%Ni−O catalysts, because the bulk NiO particles are more easier to be reduced. A similar reduction temperature of NiO was reported for TPR analysis of a Ni/Ce-ZrO_2 catalyst;[36] where the authors assigned the reduction peak at around 420 °C to the reduction of bulk NiO particles. In addition, a TPR reduction peak at around 400 °C has been reported to be attributed to the reduction of NiO particles on the outside surface of USY zeolite.[37]

In contrast, the I-series catalysts showed a different pattern of TRP reduction, where the main H_2 reduction peak was observed at around 600 °C and was a more broader peak than that found for the 10%Ni−O to 20%Ni−O catalysts. The results indicate that NiO particles on the 10%Ni−I to 20%Ni−I catalysts were much smaller compared with the O-series

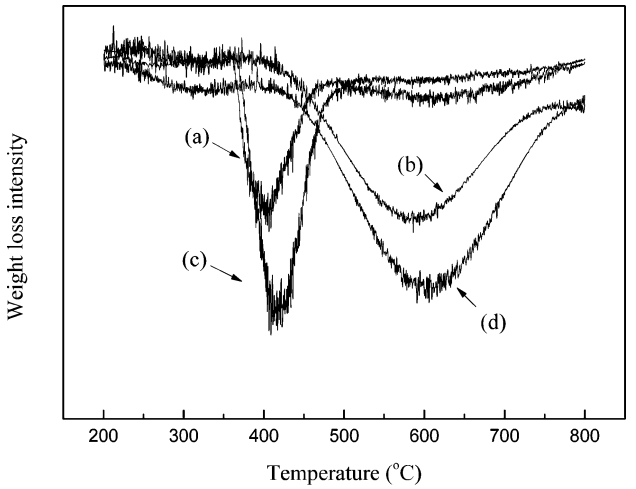

Figure 1. TPR results of fresh Ni/MCM-41 catalysts: (a) 10%Ni−O; (b) 10%Ni−I; (c) 20%Ni−O; (d) 20%Ni−I.

catalyst. Smaller metal oxide particles are known to require higher temperature for hydrogen reduction; stronger interaction between metal and support has also been reported for smaller metal particles compared with larger ones.[38,39]

By increasing the Ni loading from 10 to 20 wt % for the I and O series catalysts, the TPR peak slightly shifted to a higher temperature (Figure 1). The shift of TPR peak to higher temperature was reported for a Ni/USY catalyst with an increase of Ni loading from 5 to 9%.[37,40] The higher loading of Ni metals on the MCM-41 support might cause a delay of reduction of NiO in the TPR analysis compared with the catalyst with low nickel loading.

Bulk NiO particles with sizes up to 100 nm were observed on the freshly prepared 10%Ni−O and 20%Ni−O catalysts from SEM analysis (Figure 2a and c). The SEM micrographs shown in Figure 2, suggest that the NiO particles were deposited outside the pores of the MCM-41 support (10%Ni−O and 20% Ni−O); the SEM results are consistent with the TPR analysis where bulky NiO particles were reduced at lower temperature (410 °C). However, from the SEM analysis of the freshly prepared 10%Ni−I and 20%Ni−I catalysts (Figure 2b and d), bulk NiO particles could be barely seen on the surface. In addition, the morphology obtained for the fresh unused MCM-41 support (Figure 2e) was almost identical to the freshly prepared 10Ni−I and 20Ni−I catalysts (Figure 2b and d), suggesting that the NiO particles were not deposited on the surface, but inside the pores.

The analysis of the BET surface area of the fresh 10%Ni−O and 20%Ni−O catalysts showed that they had higher surface areas (around 870 m^2 g^{-1}) compared to the 10%Ni−I and 20% Ni−I catalysts (around 450 m^2 g^{-1}) which also supports the location of NiO particles outside or inside the pores of the MCM-41 support. It is suggested that the NiO particles for the Ni−I series of catalysts occupied the internal surfaces of the MCM-41 support, thereby reducing the surface area.

Further studies of the fresh 20%Ni−O catalysts with the TEM are shown in Figure 3, where NiO particles with particle sizes of around 50 nm were clearly observed (NiO particle compositions were confirmed from energy dispersive X-ray spectroscopy (not shown here)). However, most of the NiO particles (around 2 nm) were found inside the pores of the 20% Ni−I catalyst (Figure 2b).

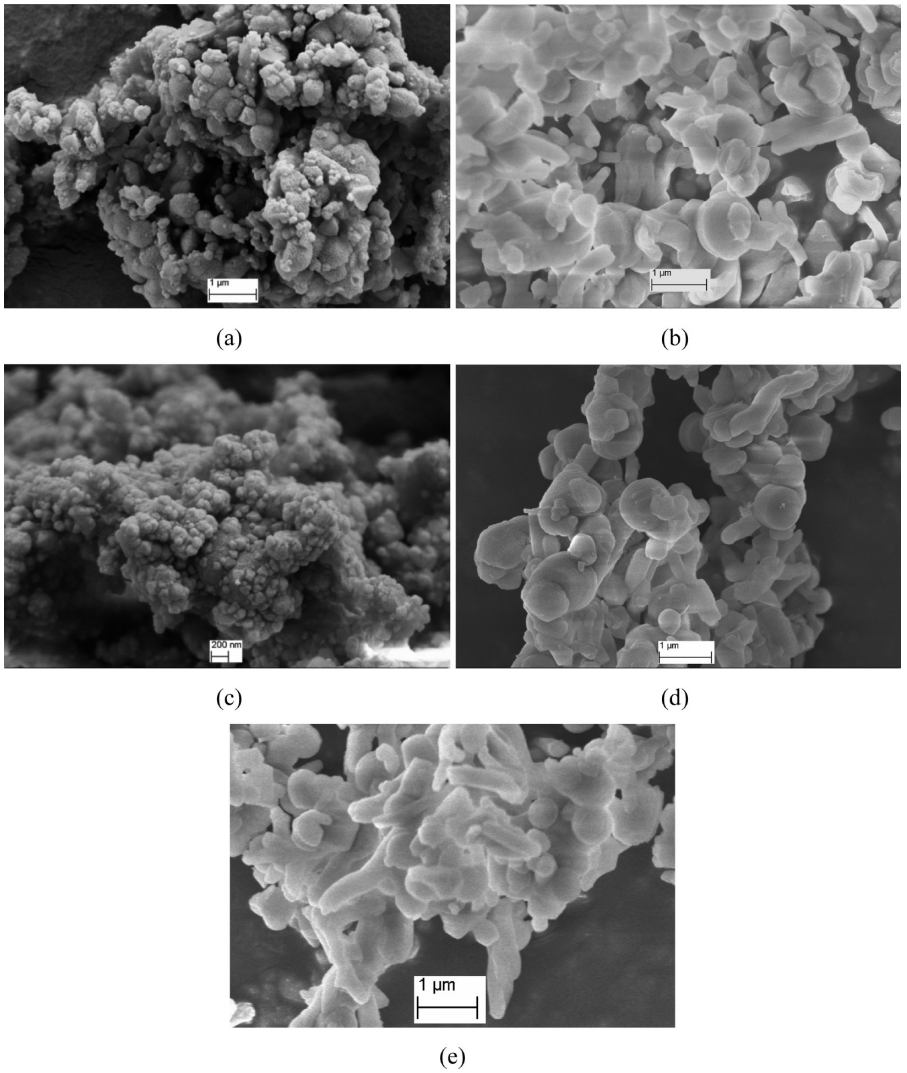

Figure 2. SEM results of fresh Ni/MCM-41 catalysts; (a) 10%Ni−O; (b) 10%Ni−I; (c) 20%Ni−O; (d) 20%Ni−I; (e) MCM-41 support.

XRD analysis was carried out on the fresh catalysts, and the results are shown in Figure 4. The XRD patterns of the 10% Ni−O and 20%Ni−O catalysts with NiO particles outside the pores of the support were found to be similar to the 40 wt % Ni/MCM-41 catalyst prepared in our previous work;[34] strong diffractions were obtained at 37°, 43°, and 64° further indicating bulk NiO particles were obtained for the 10%Ni−O and 20%Ni−O catalysts. Weak diffractions were obtained for the 10%Ni−I and 20%Ni−I catalysts, indicating that most of the NiO particles were very small and located inside the pores of the MCM-41 support.

Characterization of Reacted Catalysts. The reacted catalysts after catalytic pyrolysis/gasification of wood sawdust were analyzed by the temperature programmed oxidation (TPO) method to obtain information on the amount of coke deposition and carbon types formed on the reacted catalyst. The results of TGA−TPO are shown in Figure 5.

From the TGA−TPO results (Figure 5), a mass increase was observed at around 500 °C for each catalyst. The increase of catalyst mass was ascribed to the oxidation of Ni particles which via the in situ reduction of NiO by the produced H_2 and CO. It seems that the O-series catalysts showed a higher intensity of Ni oxidation during the TPO analysis (Figure 5a and b), compared with the I-series catalysts. Therefore, the oxidation of Ni particles during the TPO analysis was weak for the reacted 10%Ni−I and 20%Ni−I catalysts (Figure 5).

Catalysts with bulk NiO particles generate more coke during biomass gasification. The relatively high coke deposition (7 wt % of the weight of the reacted catalyst) was found on both the 10%Ni−O and 20%Ni−O catalysts as shown in Figure 5. This finding was similar to a previous report regarding heavy coke deposition observed on Ni/zeolite catalyst with a large crystal size of the NiO particles (around 25 nm).[24] The reacted 10% Ni−I catalyst where most of the NiO particles were inside the pores of the support showed the lowest level of coke deposition (Figure 5). A stronger metal support interaction has been suggested to be a reason for slow catalyst deactivation and less coke deposition on a Ni/silicate catalyst based on the dry reforming of methane.[41]

The reacted 10%Ni−I and 10%Ni−O catalysts have been analyzed by XRD (Figure 4). Ni crystals were expected (diffraction at 44° and 52°) after gasification of biomass. A broad amorphous silica peak at around 23° confirms that the structure of MCM-41 was stable after gasification experiments at 800 °C. The stable structure of the MCM-41 after experimentation is supported from the TEM analysis (Figure 3d−f). From the TEM analysis of the reacted catalyst, it appears that a slight degree of sintering has occurred, as the

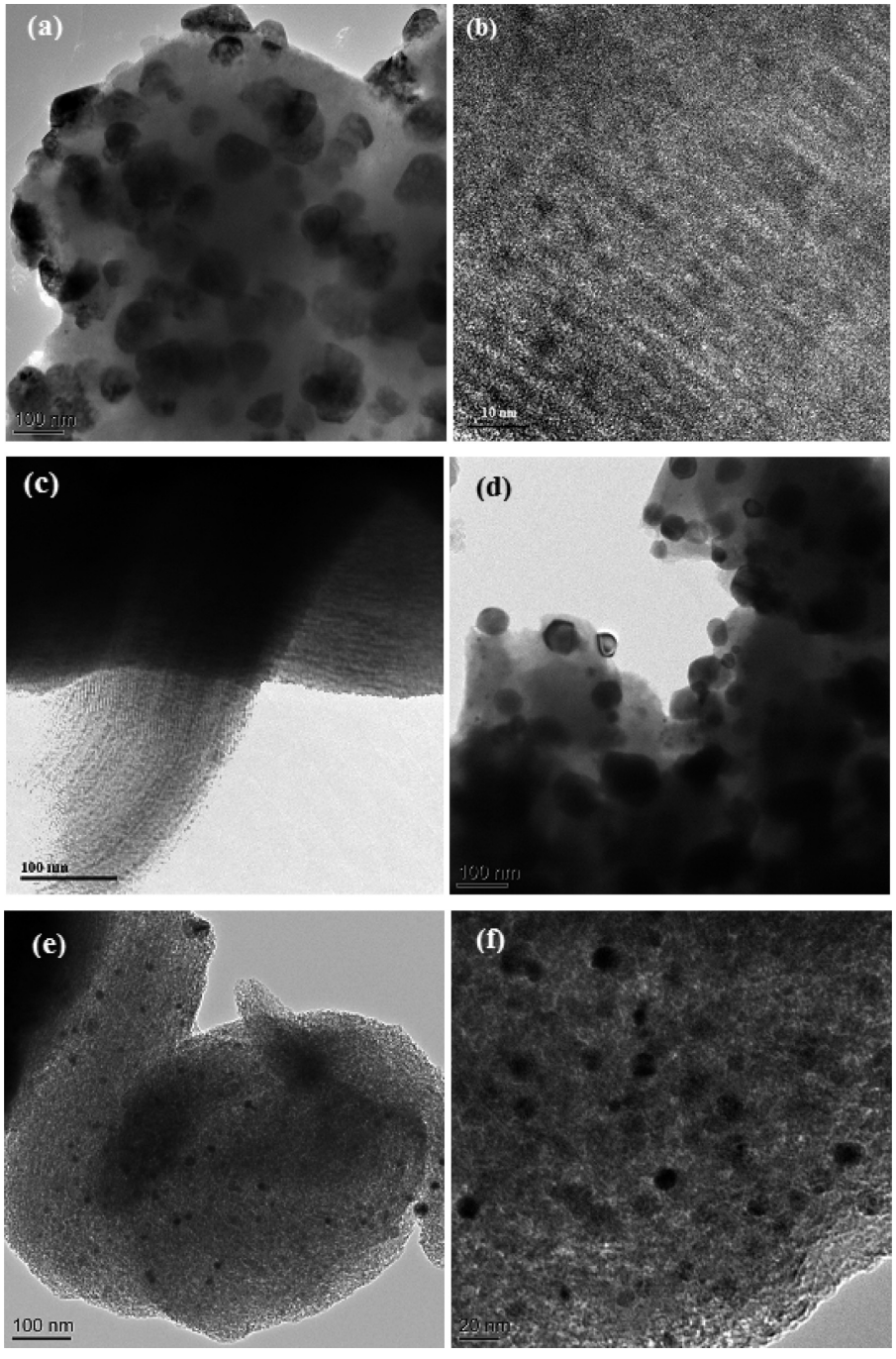

Figure 3. TEM results of Ni/MCM-41 catalysts; (a) 20%Ni−O; (b) and (c) 20%Ni−I; (d) reacted 10%Ni−O; (e) and (f) reacted 10%Ni−I.

crystal particles for the reacted 10%Ni−I catalyst were of particle sizes of around 8 nm (Figure 3f). The average crystal size of Ni particles of the reacted 10%Ni−I catalyst was also about 8 nm as calculated using the Scherrer equation from XRD analysis (Figure 4). Detailed research in relation to Ni sintering and coke deposition on the reacted catalyst is suggested to be carried out in future work to understand the performance of the Ni/MCM-41 catalyst toward commercial application.

Mass Balance of the Pyrolysis/Gasification of Wood Sawdust. The catalytic steam pyrolysis/gasification of wood sawdust was carried out with the Ni/MCM-41 catalyst with NiO particles located inside and outside the pores of the support. As shown in Table 1, the gas and hydrogen yield were increased in the presence of the Ni/MCM-41 catalyst. For example, H_2 yield, calculated as the molar of produced hydrogen divided by the mass of biomass sample, increased from ∼5 to higher than 14 mmol H_2 g^{-1} wood in the presence of the Ni/MCM-41 catalyst (Table 1). Obviously, the H_2 concentration was significantly increased with the addition of catalyst in the gasification process, while the concentrations of hydrocarbon gases showed a dramatic decrease (Table 1).

With the increase of the Ni content from 10 to 20 wt %, hydrogen production was slightly increased from 14.98 to 16.46 (mmol H_2 g^{-1} wood) for the O-series catalysts with NiO particles mostly outside the pores of the MCM-41 support but increased from 15.13 to 21.26 (mmol H_2 g^{-1} wood) for the I

dx.doi.org/10.1021/sc300133c | ACS Sustainable Chem. Eng. 2013, 1, 1083−1091

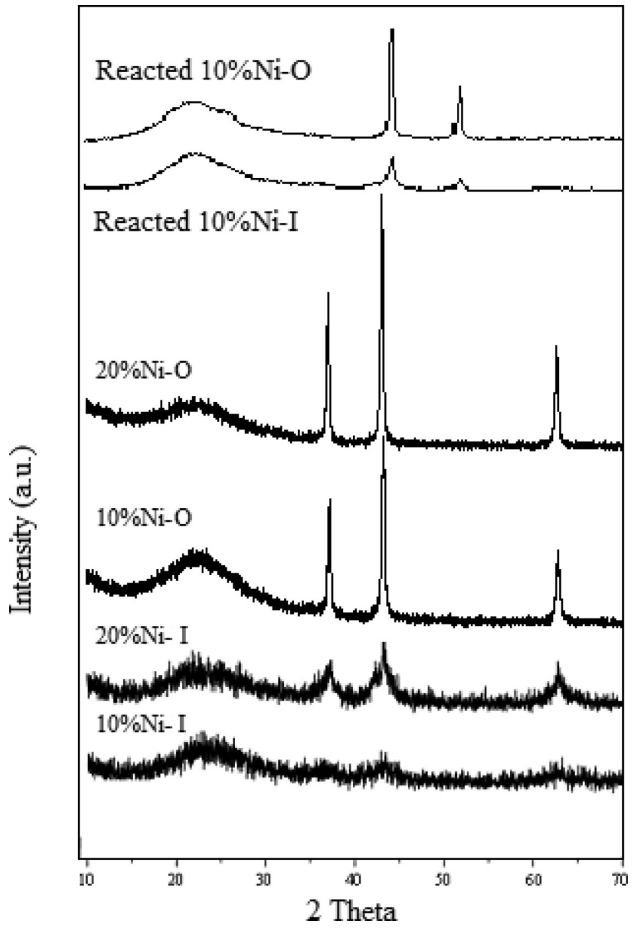

Figure 4. XRD analysis of the fresh and reacted Ni/MCM-41 catalysts.

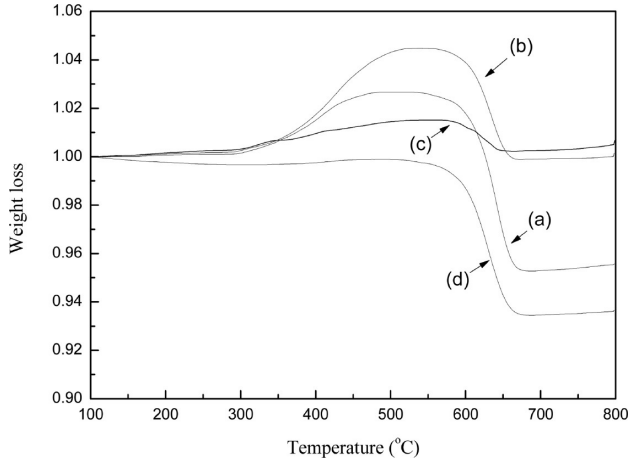

Figure 5. TGA–TPO results of reacted Ni/MCM-41 catalysts: (a) 10%Ni–O; (b) 20%Ni–O; (c) 10%Ni–I; (d) 20%Ni–I.

series catalysts with NiO particles mostly inside the pores of the catalyst support (Table 1).

By changing the location of NiO particles from mostly outside the pores (O-series catalysts) to mostly inside the pores of the support (I-series catalysts), hydrogen production and gas yield were increased. In addition, the concentration of CH_4 was reduced from 3.60 to 2.49 vol % and C_2–C_4 hydrocarbon gases were reduced from 1.32 to 0.85 vol % when the catalyst was changed from 10%Ni–O to 10%Ni–I. It was found that higher hydrogen production and a reduction in hydrocarbon gases

Table 1. Mass Balance and Gas Concentrations for the Pyrolysis/Gasification of Wood Sawdust

catalyst	sand	10% Ni–O	10% Ni–I	20% Ni–O	20% Ni–I
gas/wood (wt %)	37.01	47.91	52.17	48.61	60.80
residue/wood (wt %)	36.25	38.75	37.50	37.50	37.50
mass balance	102.81	99.75	98.00	99.96	96.35
H_2 yield (mmol H_2 g^{-1} wood)	5.14	14.98	15.13	16.46	21.26
gas concentration (vol %)					
CO	33.25	26.67	30.21	22.35	19.18
H_2	29.53	52.18	50.15	55.30	57.12
CO_2	15.13	16.23	16.29	18.63	21.22
CH_4	13.82	3.60	2.49	2.59	1.97
C_2–C_4	8.26	1.32	0.85	1.12	0.50

were obtained for the Ni/MCM-41 catalyst where most of the NiO particles were located inside the pores of the MCM-41 support. The production of hydrogen and reforming of hydrocarbon gases are mainly influenced by the following reactions:

$$CO + H_2O \leftrightarrow CO_2 + H_2 \quad (1)$$

$$CH_4 + H_2O \leftrightarrow CO + 3H_2 \quad (2)$$

$$C_nH_m + nH_2O \leftrightarrow nCO + (n + m/2)H_2 \quad (3)$$

The presence of the Ni/MCM-41 catalyst has been shown to be effective in the role of increasing hydrogen concentration and reducing the concentrations of hydrocarbon gases through reactions 1–3 (Table 1), by comparing the catalytic results with the noncatalytic experiments. Although bulky NiO particles located outside the pores of the MCM-41 support (O-series catalyst) are easily reduced during the biomass gasification (lower reduction temperature was needed from TPR analysis, Figure 1), they might be more easily deactivated due to coke deposition (Figure 5a and b). The reduced small Ni particles have a higher metal dispersion, which offers more catalytic sites for reactions 1–3 and the coke elimination reaction (reaction 4).

$$C + H_2O \leftrightarrow CO + H_2 \quad (4)$$

In contrast, the increased size of NiO particles on Ni/MCM-41 catalyst have been reported to show no increase of gas and hydrogen production due to the reduction of metal dispersion, when the Ni loading was increased during biomass gasification.[23]

GC/MS Analysis of the Oil Products. Oil products derived from the pyrolysis/gasification of wood sawdust have been analyzed using GC/MS. The GC/MS total ion chromatograms of the oil products from the noncatalytic and catalytic experiments are shown in Figure 6. The oil compounds have been quantitatively identified, and the yields are shown in Table 2.

As shown in Figure 6, similar total ion chromatograms were obtained for the analyzed oil products. In addition, numerous peaks were observed from the GC/MS analysis. It is shown that the produced oil contains a large number of oxygenated and aromatic compounds; the bio-oil is known to be complex. The largest peak observed from Figure 6 (around 12.5 min retention time) is ascribed to phenol. Phenol has been reported in the bio-oil derived from pyrolysis/gasification of biomass.[34,42,43] The other main compounds identified from the GC/MS

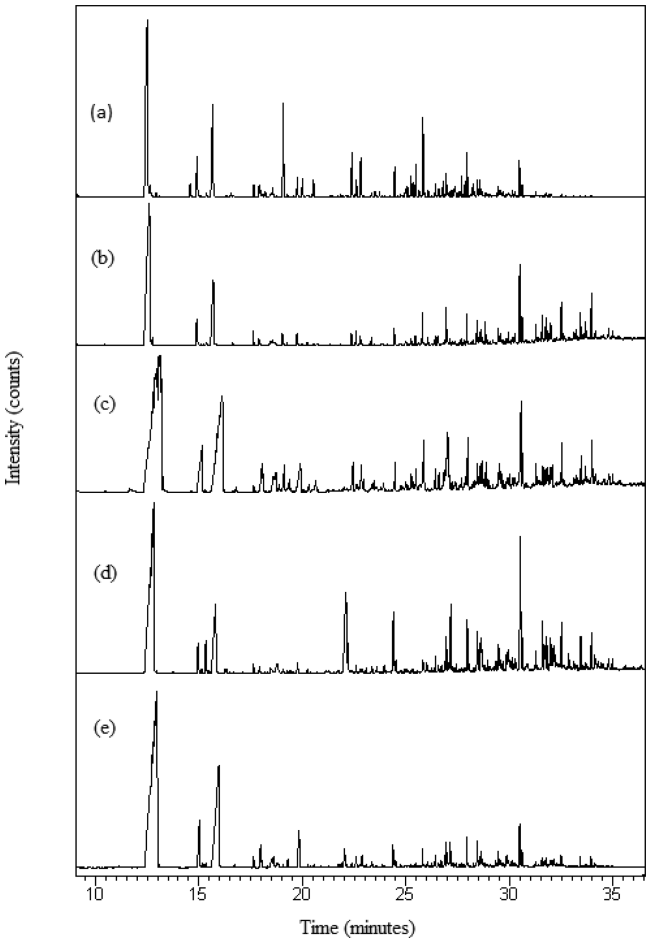

Figure 6. GC/MS graphic results of oil products from pyrolysis/gasification of biomass: (a) sand; (b) 10%Ni−O; (c) 20%Ni−O; (d) 10%Ni−I; (e) 20%Ni−I.

analysis were the following: cresol, naphthalene, phenylphenol, pyrene, etc.

As shown in Table 2, the yield of chemical compounds related to the weight of biomass sample was reduced significantly with the addition of the Ni/MCM-41 catalyst. For example, the yield of phenol was reduced from 13.7 to less than 3.5 (mg g^{-1} biomass) and cresol yield reduced from 0.64 to less than 0.13 (mg g^{-1} biomass), when the Ni/MCM-41 catalyst was added to the pyrolysis/gasification process. In addition, the total yield of identified compounds in the oil products was reduced from 18.6 to less than 3.8 (mg g^{-1} biomass) in the presence of the catalyst. The observation of reduction of oil yield was consistent with the mass balance data presented in Table 1, where gas yield and hydrogen production were significantly increased when the catalyst was introduced into the pyrolysis/gasification process. Oil reduction has been reported to be reduced during pyrolysis/gasification of municipal solid waste when Ni/Al_2O_3 catalyst was introduced into the experiment.[44] The lower oil yield in the presence of the catalyst was due to oil conversion to gaseous products (Table 1). The reduction of oil yield with the increase of Ni loading was consistent with the increased gas production shown in Table 1.

The location of the NiO particles on the surface of the MCM-41 catalyst was found to have a large influence on the oil yields from biomass gasification. For example, the total oil yield identified was around 3.8 (mg g^{-1} biomass) for the 10%Ni−O catalyst, while less than 1.3 (mg g^{-1} biomass) was obtained for the 10%Ni−I catalyst. It is indicated that the oil yield was reduced when the loading of NiO particles moved from outside to inside the pores of the MCM-41 catalyst. Therefore, the NiO particles located inside the pores of the supports are more effective for the reduction of oil compounds derived from biomass pyrolysis, resulting in a higher production of gas and hydrogen. The pore size of the I-series catalysts is around 2.9 nm (Table 1), which was much larger than the identified oil compounds; for example, the molecular size of pyrene is less than 0.9 nm.[45] The oil compounds derived from pyrolysis/gasification of wood sawdust (Table 2) could have more access to the NiO particles located inside the pores of the MCM-41 support compared with the ones outside the pores; due to the high dispersion of small NiO particles inside the large volume of the MCM-41 support compared with bulk NiO particles. The increased availability of more surface atoms in relation to smaller crystallites compared with bulk crystallites has also been reported by others.[46] Therefore, more gas and hydrogen production were obtained using the I-series catalysts where most of the NiO particles were located inside the pores compared to the O-series where the NiO particles were outside the pores.

The better performance of the I-series catalysts in relation to hydrogen production and oil reduction could also be due to the deep reactions of reforming/gasification inside the pores of the MCM-41 support. The gaseous products derived from biomass pyrolysis enter inside the MCM-41 pores and diffuse inside the pores for the I-series catalysts with longer residence time for reaction, compared with shorter reaction time on the NiO particles located outside the pores of the O-series Ni/MCM-41 catalysts. Thus the longer contact time with active Ni sites resulted in deeper reforming/gasification and higher gas and hydrogen production for the I-series catalysts (Table 1).

CONCLUSIONS

Ni/MCM-41 catalysts have been investigated for hydrogen production from the catalytic steam pyrolysis/gasification of biomass (wood sawdust). The location of NiO particles on the MCM-41 support has been manipulated to be mostly inside or outside the pores, in order to understand their catalytic performance related to hydrogen production, oil production, and coke deposition on the catalyst during the biomass gasification process.

The performance of the two types of catalyst showed that hydrogen and gas production were increased when the NiO particles were located mostly inside the mesopores of the MCM-41 support. The 10%Ni−I catalyst with most NiO particles located inside the MCM-41 support generated the lowest carbon deposition according to the TPO analysis, while coke deposition on the O-series catalysts was around 7 wt % of catalyst weight.

The higher dispersion of the smaller Ni particles inside the pores of the MCM-41 and the longer residence time of the reactants diffused inside the pores enabled increased contact with the catalytic active sites which promoted the water gas shift reaction; methane steam reaction; carbon steam reaction; and steam reforming of other hydrocarbons.

Table 2. Tentative Identified Compounds from GC/MS Analysis of the Oil Product ($\mu g\ g^{-1}$ Biomass)

RT[a] (min)	peak name	sand	10%Ni−O	10%Ni−I	20%Ni−O	20%Ni−I
12.44	phenol	13761.18	3421.75	1214.94	859.66	740.10
14.57	indene	147.21	10.33	1.51		
14.89	cresol	635.38	131.66	18.11	20.75	25.16
17.91	dimethylphenol	85.87	10.61	23.75	3.67	9.42
19.06	naphthalene	212.60	6.19	4.56	0.28	0.23
19.69	trimethylphenol			0.47		0.26
22.39	methylnaphthalene	118.50	8.06	5.97	0.18	0.34
23.85	benzofuran, methyl-	25.48				
25.09	naphthalene, ethenyl-	59.95				
25.25	dimethylnaphthalene	7.04				
25.10	naphthalene, ethenyl-	62.30				
25.47	biphenyl	11.57	0.59	3.57	0.05	0.08
25.63	naphthalene, dimethyl-	55.15	2.09	0.71	0.04	0.11
25.67	naphthalene, dimethyl-	29.48	0.72	0.45	0.07	0.08
25.82	acenaphthylene	32.48	3.01			
26.94	dibenzofuran	49.80	20.67	0.18	1.00	0.41
26.58	biphenyl, methyl-	2.68				
27.15	naphthalene, trimethyl	17.57				
27.50	biphenyl, methyl-	2.75				
28.23	fluorene	550.71	5.52	3.89	4.87	2.10
28.83	diphenylpropane	16.39	4.54	0.88	0.14	0.07
29.46	phenylphenol	1797.82	21.70	1.82	2.24	1.69
29.68	fluorene, methyl-	63.87				
30.48	phenanthrene	251.45	45.46	3.93	8.40	3.78
31.29	phenylnaphthalene	0.00	0.00	0.60	0.69	0.00
31.72	anthracene, methyl-	18.57	50.92	0.00	11.79	2.39
31.79	phenanthrene, methyl-	33.70				
33.41	fluoranthene		35.30	3.28	5.14	6.32
33.94	pyrene	530.74	57.45	4.90	5.70	4.33
total		18580.23	3836.54	1293.52	924.67	796.86

[a]RT−retention time; for each experiment, retention time is slightly different.

AUTHOR INFORMATION

Corresponding Author

*Tel.: 44 1133432504. E-mail: p.t.williams@leeds.ac.uk (P.T.W.); c.wu@leeds.ac.uk (C.W.). Tel.: 61 2 9351 7483. E-mail: jun.huang@sydney.edu.au (J.H.).

Notes

The authors declare no competing financial interest.

ACKNOWLEDGMENTS

This work was supported by the International Exchange Scheme from the Royal Society (IE110273) and the Early Career Research Scheme from the University of Sydney.

REFERENCES

(1) Seth, D. Hydrogen futures: toward a sustainable energy system. *Int. J. Hydrogen Energy* **2002**, *27* (3), 235−264.

(2) Urbaniec, K.; Friedl, A.; Huisingh, D.; Claassen, P. Hydrogen for a sustainable global economy. *J. Cleaner Prod.* **2010**, *18* (Supplement 1 (0)), S1−S3.

(3) Krishnan, P.; Hsueh, K.-L.; Yim, S.-D. Catalysts for the hydrolysis of aqueous borohydride solutions to produce hydrogen for PEM fuel cells. *Appl. Catal. B: Environ.* **2007**, *77* (1−2), 206−214.

(4) Li, J.; Han, Y.; Zhu, Y.; Zhou, R. Purification of hydrogen from carbon monoxide for fuel cell application over modified mesoporous CuO−CeO2 catalysts. *Appl. Catal. B: Environ.* **2011**, *108−109* (0), 72−80.

(5) Balat, M.; Balat, M. Political, economic and environmental impacts of biomass-based hydrogen. *Int. J. Hydrogen Energy* **2009**, *34* (9), 3589−3603.

(6) Eurostat *Renewable energy statistics*; Luxembourg, 2011.

(7) EU *EU Climate and Energy Package*; Brussels, 2009.

(8) *UK biomass strategy*; Department for Environment, Food and Rural Affairs: London, 2007.

(9) Gao, N.; Li, A.; Quan, C. A novel reforming method for hydrogen production from biomass steam gasification. *Bioresour. Technol.* **2009**, *100* (18), 4271−4277.

(10) Gao, N.; Li, A.; Quan, C.; Gao, F. Hydrogen-rich gas production from biomass steam gasification in an updraft fixed-bed gasifier combined with a porous ceramic reformer. *Int. J. Hydrogen Energy* **2008**, *33* (20), 5430−5438.

(11) Lv, P.; Yuan, Z.; Ma, L.; Wu, C.; Chen, Y.; Zhu, J. Hydrogen-rich gas production from biomass air and oxygen/steam gasification in a downdraft gasifier. *Renewable Energy* **2007**, *32* (13), 2173−2185.

(12) de Vlieger, D. J. M.; Chakinala, A. G.; Lefferts, L.; Kersten, S. R. A.; Seshan, K.; Brilman, D. W. F. Hydrogen from ethylene glycol by supercritical water reforming using noble and base metal catalysts. *Appl. Catal. B: Environ.* **2012**, *111−112* (0), 536−544.

(13) Basagiannis, A. C.; Verykios, X. E. Catalytic steam reforming of acetic acid for hydrogen production. *Int. J. Hydrogen Energy* **2007**, *32* (15), 3343−3355.

(14) Trane, R.; Dahl, S.; Skjøth-Rasmussen, M. S.; Jensen, A. D. Catalytic steam reforming of bio-oil. *Int. J. Hydrogen Energy* **2012**, *37* (8), 6447−6472.

(15) Davda, R. R.; Shabaker, J. W.; Huber, G. W.; Cortright, R. D.; Dumesic, J. A. Aqueous-phase reforming of ethylene glycol on silica-supported metal catalysts. *Appl. Catal. B: Environ.* **2003**, *43* (1), 13−26.

(16) Vagia, E. C.; Lemonidou, A. A. Investigations on the properties of ceria−zirconia-supported Ni and Rh catalysts and their performance in acetic acid steam reforming. *J. Catal.* **2010**, *269* (2), 388−396.

(17) Garcia, L. a.; French, R.; Czernik, S.; Chornet, E. Catalytic steam reforming of bio-oils for the production of hydrogen: effects of catalyst composition. *Appl. Catal. A: Gen.* **2000**, *201* (2), 225−239.
(18) Davidian, T.; Guilhaume, N.; Iojoiu, E.; Provendier, H.; Mirodatos, C. Hydrogen production from crude pyrolysis oil by a sequential catalytic process. *Appl. Catal. B: Environ.* **2007**, *73* (1−2), 116−127.
(19) Furusawa, T.; Tsutsumi, A. Comparison of Co/MgO and Ni/MgO catalysts for the steam reforming of naphthalene as a model compound of tar derived from biomass gasification. *Appl. Catal. A: Gen.* **2005**, *278* (2), 207−212.
(20) Park, H. J.; Park, S. H.; Sohn, J. M.; Park, J.; Jeon, J.-K.; Kim, S.-S.; Park, Y.-K. Steam reforming of biomass gasification tar using benzene as a model compound over various Ni supported metal oxide catalysts. *Bioresour. Technol.* **2010**, *101* (1, Supplement), S101−S103.
(21) Isoda, T.; Nakahara, T.; Kusakabe, K.; Morooka, S. Catalytic Cracking of Polyethylene-Liquefied Oil over Amorphous Aluminosilicate Catalysts. *Energy Fuels* **1998**, *12* (6), 1161−1167.
(22) Wu, C.; Williams, P. T. Hydrogen production by steam gasification of polypropylene with various nickel catalysts. *Appl. Catal. B: Environ.* **2009**, *87* (3−4), 152−161.
(23) Zhao, M.; Florin, N. H.; Harris, A. T. The influence of supported Ni catalysts on the product gas distribution and H2 yield during cellulose pyrolysis. *Appl. Catal. B: Environ.* **2009**, *92* (1−2), 185−193.
(24) Inaba, M.; Murata, K.; Saito, M.; Takahara, I. Hydrogen Production by Gasification of Cellulose over Ni Catalysts Supported on Zeolites. *Energy Fuels* **2006**, *20* (2), 432−438.
(25) Buchireddy, P. R.; Bricka, R. M.; Rodriguez, J.; Holmes, W. Biomass Gasification: Catalytic Removal of Tars over Zeolites and Nickel Supported Zeolites. *Energy Fuels* **2010**, *24* (4), 2707−2715.
(26) Yan-ping, Q. I.; Sheng-li, C.; Peng, D.; Ke-qi, X. U.; Bao-jian, S. Novel macroporous residua FCC catalysts. *J. Fuel Chem. Technol.* **2006**, *34* (6), 685−690.
(27) Lau, S. H.; Caps, V.; Yeung, K. W.; Wong, K. Y.; Tsang, S. C. A novel MCM-41-supported manganese(III) complex with nitrogen donor ligand for cyclohexene oxidation. *Microporous Mesoporous Mater.* **1999**, *32* (3), 279−285.
(28) Paulino, I. S.; Schuchardt, U. Ethylene polymerization using iron catalysts heterogenized in MCM-41. *Catal. Commun.* **2004**, *5* (1), 5−7.
(29) Du, G.; Lim, S.; Yang, Y.; Wang, C.; Pfefferle, L.; Haller, G. L. Methanation of carbon dioxide on Ni-incorporated MCM-41 catalysts: The influence of catalyst pretreatment and study of steady-state reaction. *J. Catal.* **2007**, *249* (2), 370−379.
(30) Jentys, A.; Pham, N. H.; Vinek, H.; Englisch, M.; Lercher, J. A. Synthesis and characterization of mesoporic materials containing highly dispersed cobalt. *Microporous Mater.* **1996**, *6* (1), 13−17.
(31) Jentys, A.; Pham, N. H.; Vinek, H.; Englisch, M.; Lercher, J. A. Structure of Co and Co oxide clusters in MCM-41. *Catal. Today* **1998**, *39* (4), 311−315.
(32) Khodakov, A. Y.; Griboval-Constant, A.; Bechara, R.; Villain, F. Pore-Size Control of Cobalt Dispersion and Reducibility in Mesoporous Silicas. *J. Phys. Chem. B* **2001**, *105* (40), 9805−9811.
(33) Khodakov, A. Y.; Griboval-Constant, A.; Bechara, R.; Zholobenko, V. L. Pore Size Effects in Fischer−Tropsch Synthesis over Cobalt-Supported Mesoporous Silicas. *J. Catal.* **2002**, *206* (2), 230−241.
(34) Wu, C.; Wang, L.; Williams, P. T.; Shi, J.; Huang, J. Hydrogen production from biomass gasification with Ni/MCM-41 catalysts: Influence of Ni content. *Appl. Catal. B: Environ.* **2011**, *108−109* (0), 6−13.
(35) Cheng, C.-F.; Ho Park, D.; Klinowski, J. Optimal parameters for the synthesis of the mesoporous molecular sieve [Si]-MCM-41. *J. Chem. Soc., Faraday Trans.* **1997**, *93* (1), 193−197.
(36) Dong, W.-S.; Roh, H.-S.; Jun, K.-W.; Park, S.-E.; Oh, Y.-S. Methane reforming over Ni/Ce-ZrO2 catalysts: effect of nickel content. *Appl. Catal. A: Gen.* **2002**, *226* (1−2), 63−72.
(37) Pawelec, B.; Daza, L.; Fierro, J. L. G.; Anderson, J. A. Regeneration of Ni-USY catalysts used in benzene hydrogenation. *Applied Catalysis A: General* **1996**, *145* (1−2), 307−322.
(38) Khodakov, A. Y.; Lynch, J.; Bazin, D.; Rebours, B.; Zanier, N.; Moisson, B.; Chaumette, P. Reducibility of Cobalt Species in Silica-Supported Fischer−Tropsch Catalysts. *J. Catal.* **1997**, *168* (1), 16−25.
(39) Bechara, R.; Balloy, D.; Dauphin, J.-Y.; Grimblot, J. Influence of the Characteristics of γ-Aluminas on the Dispersion and the Reducibility of Supported Cobalt Catalysts. *Chem. Mater.* **1999**, *11* (7), 1703−1711.
(40) Hoffer, B. W.; Dick van Langeveld, A.; Janssens, J.-P.; Bonné, R. L. C.; Lok, C. M.; Moulijn, J. A. Stability of highly dispersed Ni/Al2O3 catalysts: Effects of pretreatment. *J. Catal.* **2000**, *192* (2), 432−440.
(41) Frontera, P.; Macario, A.; Aloise, A.; Crea, F.; Antonucci, P. L.; Nagy, J. B.; Frusteri, F.; Giordano, G. Catalytic dry-reforming on Ni−zeolite supported catalyst. *Catal. Today* **2012**, *179* (1), 52−60.
(42) Gilbert, P.; Ryu, C.; Sharifi, V.; Swithenbank, J. Tar reduction in pyrolysis vapours from biomass over a hot char bed. *Bioresour. Technol.* **2009**, *100* (23), 6045−6051.
(43) Phuphuakrat, T.; Nipattummakul, N.; Namioka, T.; Kerdsuwan, S.; Yoshikawa, K. Characterization of tar content in the syngas produced in a downdraft type fixed bed gasification system from dried sewage sludge. *Fuel* **2010**, *89* (9), 2278−2284.
(44) Blanco, P. H.; Wu, C.; Onwudili, J. A.; Williams, P. T. Characterization of Tar from the Pyrolysis/Gasification of Refuse Derived Fuel: Influence of Process Parameters and Catalysis. *Energy Fuels* **2012**, *26* (4), 2107−2115.
(45) Martinho, J. M. G.; Winnik, M. A. Transient effects in pyrene monomer-excimer kinetics. *J. Phys. Chem.* **1987**, *91* (13), 3640−3644.
(46) Kurr, P.; Kasatkin, I.; Girgsdies, F.; Trunschke, A.; Schlögl, R.; Ressler, T. Microstructural characterization of Cu/ZnO/Al2O3 catalysts for methanol steam reforming—A comparative study. *Appl. Catal. A: Gen.* **2008**, *348* (2), 153−164.